Dalton Transactions

RSC Publishing

PAPER

View Article Online
View Journal | View Issue

Cite this: *Dalton Trans.*, 2013, **42**, 9877

AIE luminogen bridged hollow hydroxyapatite nanocapsules for drug delivery†

Dongdong Li,[a] Zhiqiang Liang,[a] Jie Chen,[b] Jihong Yu*[a] and Ruren Xu[a]

A new type of organophosphonic acid, (4,4′-(1,2-diphenylethene-1,2-diyl)bis(4,1-phenylene))bis(methylene)diphosphonic acid (PATPE), based on tetraphenylethene has been prepared, and its ester derivative exhibits the characteristic property of aggregation-induced emission (AIE) in DMSO–H_2O solution. The PATPE is then fabricated into hydroxyapatite by a one-pot condensation process to form hollow mesoporous nanocapsules of ellipsoidal morphology. The AIE luminogen-bridged hollow hydroxyapatite nanocapsules emit strong blue light under UV irradiation, which is further used for drug delivery using ibuprofen (IBU) as a model drug. The fluorescence intensity of the materials varies greatly with the loading and release of IBU, suggesting that the drug release process may be tracked in terms of the change of luminescence intensity. The biocompatibility of AIE luminogen functionalized material is also evaluated on HUH7 human hepatoma cells using the MTT assay. The low cytotoxicity of the materials reveals that the as-prepared multifunctional hydroxyapatite will be a new candidate for simultaneous drug delivery and cell imaging in potential bioapplications.

Received 24th January 2013,
Accepted 22nd April 2013

DOI: 10.1039/c3dt50243k

www.rsc.org/dalton

1. Introduction

Mesoporous materials, which have tunable pore size, large specific surface area and internal volume, have become a class of promising material for immobilization of biologically active species, especially drug molecules.[1–4] So far, many types of mesoporous materials including silica,[5] phosphates,[6] carbon,[7] and so on,[8] have been employed for drug loading. Among these materials, hydroxyapatite (HAp, $Ca_{10}(PO_4)_6(OH)_2$), the main inorganic component of natural bone, has been intensively studied as the drug delivery system, owing to its good biological compatibility and surface properties.[9] Up to now, many works have been reported about the drug storage/release systems based on mesoporous HAp, which show great advantage in efficiently enhancing drug loading and slowing down the release rate.[10,11]

Recently, the design and synthesis of luminescent functionalized mesoporous materials have attracted more and more attentions for their application in imaging guided therapy. Several types of fluorescent nanomaterials have been introduced into mesoporous materials for biomedical imaging,[12,13] such as semiconductor quantum dots (QDs),[14] metal nanoclusters,[15] metal ions,[16] organic dyes,[17,18] *etc.* Among these materials, the high concentration of QDs may cause serious problems such as enhanced cytotoxicity, which limits their further application in the area of living marking or imaging.[19] On the other hand, when more luminescent organic dyes, such as rhodamine, fluorescein, and nile red are incorporated into the solid materials, their emissions will be weakened due to the notorious aggregation-caused quenching (ACQ) effect.[20] Since the first anti-ACQ materials namely aggregation-induced emission (AIE) were found by Tang and coworkers,[21] they have aroused considerable attention because of their striking turn-on fluorescence phenomenon mainly caused by restriction of intramolecular rotation in the aggregation state.[22,23] These materials have been incorporated in silica nanoparticles and polymers, and used as fluorescent probes in intracellular imaging.[24–26] More recently, we have introduced AIE luminogen tetraphenylethene (TPE) into mesoporous SBA-15 through post-grafting methods.[27,28] The synthesized materials combine the unique properties of the AIE luminogen and porous materials, proving to be excellent fluorescence probes for potential applications in drug delivery and explosive detection.

In the present study, we have prepared mesoporous HAp with (4,4′-(1,2-diphenylethene-1,2-diyl)bis(4,1-phenylene))bis(methylene)diphosphonic acid (PATPE) containing AIE-active molecule TPE by a one-pot condensation process. Namely, PATPE molecules are incorporated in the three-dimensional network structure of HAp through P–O–Ca covalent bonds.

[a]*State Key Laboratory of Inorganic Synthesis and Preparative Chemistry, College of Chemistry, Jilin University, Changchun, 130012, P. R. China. E-mail: jihong@jlu.edu.cn; Fax: +86 431 85168608; Tel: +86 431 85168608*

[b]*Key Laboratory of Polymer Ecomaterials, Changchun Institute of Applied Chemistry, Chinese Academy of Sciences, Changchun, 130022, P. R. China*

†Electronic supplementary information (ESI) available: Details of SEM, IR. See DOI: 10.1039/c3dt50243k

The obtained AIE luminogen-bridged mesoporous HAp materials exhibit ellipsoidal hollow nanocapsule morphology, and show strong fluorescence property and good biocompatibility. The drug loading and release process can also be monitored by the change of luminescence intensity, showing great advantage over other traditional materials. The results suggest that this multifunctional material may be used as an excellent drug carrier and the drug release process can be tracked by the change of luminescence intensity in future bioapplications.

2. Materials and methods

2.1 Materials

Cetyltrimethylammonium bromide (CTAB, Shanghai Huishi Chemical Co., Ltd.), $(NH_4)_2HPO_4$ (Beijing Beihua Chemical Co., Ltd.), $Ca(NO_3)_2{\cdot}4H_2O$ (Tianjin Guangfu Chemical Regent Co., Ltd.), ibuprofen (IBU, Nanjing Chemical Regent Co., Ltd.), triethyl phosphite (Chengdu Kelong Chemical Regent Co., Ltd.). All the initial chemicals in this work were used without further purification, except THF was distilled from sodium under nitrogen in the presence of benzophenone. 1,2-Bis-[4-(bromomethyl)phenyl]-1,2-diphenylethene (BTPE) was prepared according to the reported procedures.[29]

2.2 Preparation of tetraethyl(4,4′-(1,2-diphenylethene-1,2-diyl)bis(4,1-phenylene))bis(methylene)diphosphonate (PETPE)

BTPE (1.55 g, 3 mmol) was added to triethyl phosphite (10 mL), and the resulting solution was refluxed for about 12 h. After solvent evaporation under reduced pressure, the residue was purified by column chromatography on silica gel (ethyl acetate). Yield: 1.1 g (58%). ^{1}H NMR (300 MHz, $CDCl_3$): δ 7.08 (m, 18H), 3.95 (m, 8H), 3.04 (d, 4H), 1.20 (m, 12H). ^{13}C NMR (75 MHz, $CDCl_3$): 143.6, 142.1, 140.5, 131.4, 131.2, 129.5, 129.2, 127.6, 126.4, 62.1, 34.5, 32.7, 16.3. HRMS (micrOTOF): m/z calcd for $C_{36}H_{42}O_6P_2$: 633.2529 $[M + H]^+$; found: 633.2509.

2.3 Preparation of (4,4′-(1,2-diphenylethene-1,2-diyl)bis-(4,1-phenylene))bis(methylene)diphosphonic acid (PATPE)

PETPE (0.7 g, 1.1 mmol) and $(CH_3)_3SiBr$ (0.87 mL, 6.6 mmol) were dissolved in CH_2Cl_2 (30 mL) and stirred at room temperature for about 24 h, then the solvent was removed and MeOH (20 mL) was added with stirring for 2 h. The solvent was removed under reduced pressure and washed with CH_2Cl_2 thoroughly. The product was obtained as a yellow solid (0.57 g, 100%). ^{1}H NMR (300 MHz, DMSO): δ 7.06 (m, 18H), 2.90 (d, 4H). ^{13}C NMR (75 MHz, DMSO): 142.9, 141.2, 140.5, 131.8, 130.5, 130.2, 129.1, 127.8, 125.4, 35.5, 33.7. HRMS (micrOTOF): m/z calcd for $C_{28}H_{26}O_6P_2$: 519.1126 $[M - H]^-$; found: 519.1086.

2.4 Synthesis of mesoporous HAp hybrid with AIE luminogen PATPE

CTAB (0.2 g, 0.55 mmol) was dissolved in deionized water (5 mL) containing $Ca(NO_3)_2{\cdot}4H_2O$ (1.28 g, 5.42 mmol), then the solution was adjusted to pH = 10 using $NH_3{\cdot}H_2O$ and kept at 40 °C water bath with stirring for about 1 h. $(NH_4)_2HPO_4$ (0.43 g, 3.25 mmol) and PATPE (0.073 g, 0.14 mmol) were added to water (5 mL) and the pH was adjusted to 10 with $NH_3{\cdot}H_2O$. Subsequently, the latter solution was added dropwise to the former solution containing CTAB and $Ca(NO_3)_2$, yielding a milky suspension, which was continue to be stirred at 40 °C for 2 h. The obtained mixture was transferred to a Teflon-lined autoclave and crystallized statically at 80 °C under autogenous pressure for about 24 h. The obtained precipitate was filtered off and washed several times with deionized water, DMSO and ethanol, and then refluxed in ethanol for 24 h to remove the template. After drying at 60 °C, the material functionalized with the AIE luminogen (PATPE), marked as MHAp-FL, was obtained. The pure mesoporous HAp (MHAp) was synthesized using the same method without adding PATPE.

2.5 *In vitro* drug release and fluorescence spectra

The drug storage and *in vitro* release experiment using MHAp-FL as a carrier was carried out as follows: MHAp-FL sample (0.1 g) was dried at 80 °C for about 6 h and then was added to hexane solution (15 mL) containing 60 mg mL^{-1} ibuprofen. The resulting mixture was stirred in a vial for 24 h and sealed to prevent the evaporation of organic solvent. Then the material was centrifuged and fully dried at 60 °C in air, marked as MHAp-FL-IBU. The amount of IBU adsorbed onto the MHAp-FL was determined by thermogravimetry (TG) analysis. Several samples of MHAp-FL-IBU of the same quality were put into simulated body fluid (SBF) (142.0/5.0/2.5/1.5/147.8/4.2/1.0/0.5 = $Na^+/K^+/Ca^{2+}/Mg^{2+}/Cl^-/HCO_3^-/HPO_4^{2-}/SO_4^{2-}$) (pH 7.4) at 37 °C under slow stirring, respectively. The volume of SBF was determined by IBU adsorbed to the materials with the ratio of 1 mL mg^{-1}. After the IBU was released for a specific time, the samples were centrifuged and dried. Then the samples were filled into the circular groove, compacted as much as possible and the fluorescence intensity of these samples was tested under the same conditions (slit width, voltage, *etc.*). The percentage of drug release at different times can be obtained by UV-vis analysis at 220 nm. The release system of MHAp was prepared through the same process.

2.6 Cell viability (MTT assay)

To evaluate the biocompatibility of the MHAp and MHAp-FL, cell viability was investigated using the method based on the MTT assay which is a standard test for screening the toxicity of biomaterials. Typically, MHAp-FL powder (300 mg) was added into a glass bottle and sterilized by ultraviolet irradiation for 0.5 h, then Dulbecco's modified Eagle's medium (DMEM) (3 mL) containing 10% fetal bovine serum (FBS) culture medium was added, incubated at 37 °C for 24 h and filtered. HUH7 human hepatoma cells were cultured in DMEM medium with 10% FBS at 37 °C under a humidified atmosphere containing 5% CO_2, the cell culture medium changed once every other day until reached 95% confluence, then the cells were trypsinized with buffered saline solution containing 0.25% trypsin. After that, the cells were placed in a 96-well plate at a density of 1.0×10^4 cells per well. Then the extract solution was diluted to a specific concentration of 0.2, 0.3, 0.6,

1.3, 2.5, 5, 10, 20 and 40 mg mL^{-1}, respectively and immediately added into the cells with incubation for 24 h at 37 °C. The culture medium and 20 μL MTT solution (5 mg mL^{-1}) were added to each well. After cultured for 4 hours, the culture medium was removed and 150 μL of DMSO was added to each well, and then the plate was placed on a shaking table for about 10 min, and the absorbance of the suspension was measured at 492 nm.

2.7 Characterizations

Powder X-ray diffraction (XRD) patterns were recorded on a Rigaku D/MAX 2500/PC X-ray diffractometer with CuKα radiation (λ = 0.15405 nm). N_2 adsorption–desorption isotherms were measured on a Micromeritics ASAP 2010 M apparatus at 77 K. Surface areas were estimated according to the Brunauer–Emmett–Teller (BET) method, and the pore-size distributions were calculated based on the adsorption branch of the isotherm with Barrett–Joyner–Halenda (BJH) method. Transmission-electron-microscopy (TEM) images were recorded with a Tecnai F20 electron microscope. CHN elemental analyses were carried out on a varioMICRO elemental analyzer. Infrared (IR) measurements of the samples dispersed in KBr pellets were performed on a Perkin-Elmer spectrum 430 FT-IR spectrometer. UV-Vis adsorption spectra were obtained on a Shimadzu UV-2550 spectrophotometer. The photoluminescence (PL) emission spectra were obtained on a Shimadzu RF-5301PC spectrofluorometer. Thermogravimetric (TG) measurement was produced by a TGA Q500 system in air with a heating rate of 10 K min^{-1}.

3. Results and discussion

The compound PETPE was prepared according to the synthetic route shown in Scheme 1. To investigate the AIE property of PETPE, we added different amounts of water, a poor solvent for the luminogen, to its pure DMSO solutions (3×10^{-5} mol L^{-1}) and monitored the PL changes (Fig. 1). The PL intensity of PETPE increases slowly when the volume fraction of water is lower than 60%, while increases dramatically when more water was added. The mixture emits intense blue light with the PL peak centered at 475 nm. The PL intensities increase by 106 fold from the pure DMSO solution to DMSO–H_2O mixture with 90% water.

The PATPE molecules were introduced into HAp through P–O–Ca covalent bonds by a one-pot condensation process by using CTAB as the surfactant. After removing the surfactant, the material functionalized with the AIE luminogen was obtained, marked as MHAp-FL. The content of PATPE introduced in MHAp-FL determined by elemental analysis was 0.09 mmol g^{-1} (Table 1). Fig. 2 shows the representative wide angle XRD patterns of MHAp-FL, and pure mesoporous HAp (MHAp) as compared with the standard data for hydroxyapatite. All the materials display typical diffraction peaks of HAp, which are consistent with the standard database (JCPDS No. 09-0432), indicating that the obtained samples are HAp crystals. However, the slight increase of the peak broadening of MHAp-FL suggests a modest increase of structural disorder.[30]

Fig. S1† presents the typical SEM images of as-synthesized MHAp and MHAp-FL samples. It can be seen from Fig. S1a† that MHAp are mostly uniform rod-like nanoparticles with

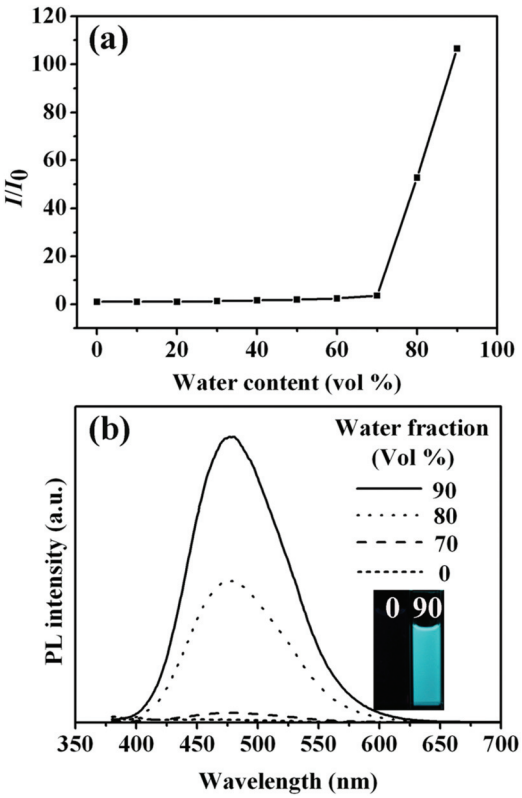

Fig. 1 (a) Plot of I/I_0 values *versus* the compositions of aqueous mixtures, I_0 = emission intensity in pure DMSO solution. (b) PL spectra changes of PETPE depending on the water fractions in DMSO. Excitation wavelength: 360 nm. Inset shows the fluorescence emission of PETPE taken under the UV light (365 nm).

Table 1 Textural parameters of MHAp, MHAp-FL, and MHAp-FL-IBU samples

Samples	V (cm^3 g^{-1})	S_{BET} (m^2 g^{-1})	D_{BJH} (nm)	IBU (wt%)	PATPE (mmol g^{-1})
MHAp	0.16	42.0	2	24	—
MHAp-FL	0.32	119.7	2–30	73	0.09
MHAp-FL-IBU	0.14	51.5	2–30	—	—

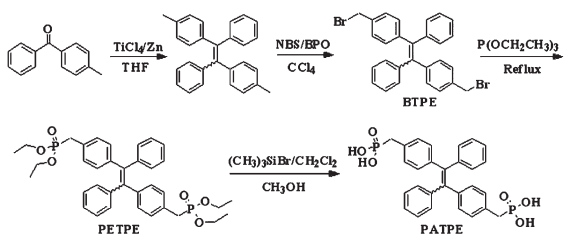

Scheme 1 The synthetic route of PETPE and PATPE.

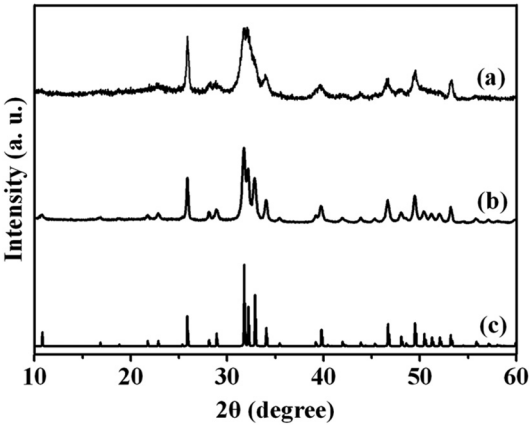

Fig. 2 Wide angle XRD patterns of (a) MHAp-FL, (b) MHAp, (c) the standard data for HAp.

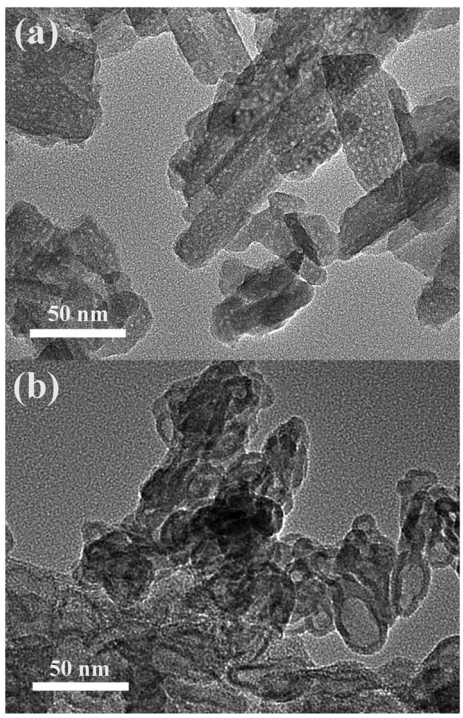

Fig. 3 TEM images of (a) MHAp, (b) MHAp-FL.

average diameter of 20–40 nm in width and 100–200 nm in length. When doped with PATPE, the particle size of MHAp-FL has been greatly reduced with a length of about 50 nm (Fig. S1b†). The difference in crystal dimension as well as shape may be attributed to the introduction of PATPE during the synthesis of MHAp-FL.

The TEM images of MHAp and MHAp-FL are shown in Fig. 3, which provide fine details of the crystal morphology and the pore information. It is found that the pores of MHAp are irregular with an average pore size of 2–5 nm. Interestingly, the MHAp-FL exhibits ellipsoidal hollow nanocapsule morphology with the pore size of 2–30 nm. Obviously, introducing

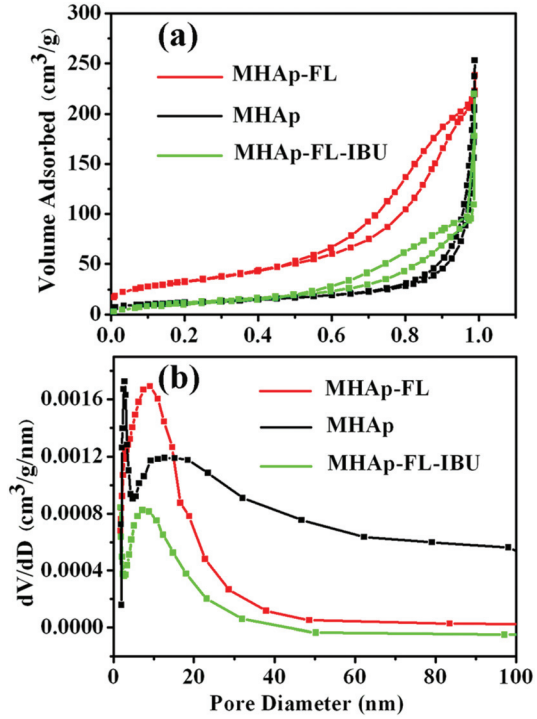

Fig. 4 (a) N_2 adsorption/desorption isotherms of MHAp-FL, MHAp, and MHAp-FL-IBU, respectively. (b) Corresponding pore size distributions based on the adsorption branch of the isotherm with the Barrett–Joyner–Halenda (BJH) method.

PATPE to MHAp expands the pore size of the resulting materials.

The N_2 adsorption–desorption isotherms and pore size distributions of MHAp, MHAp-FL and MHAp-FL-IBU are shown in Fig. 4. The BET surface area and pore volume of MHAp are 42 $m^2\ g^{-1}$ and 0.16 $cm^3\ g^{-1}$, respectively, and the pore size distribution is between 2 and 5 nm, in agreement with the TEM observation. Besides the well-defined mesopores, this material shows interparticle (textural) porosity with the pore size distribution at 5–30 nm as evidenced by the adsorption step at high relative pressures of >0.9 (Fig. 4a). While MHAp-FL shows similar IV isotherm and typical H1 hysteresis loops when P/P_0 is over 0.5, revealing the typical character of mesoporous materials. The respective BET surface area, pore volume, and pore size of MHAp-FL are 120 $m^2\ g^{-1}$, 0.32 $cm^3\ g^{-1}$, and 2–30 nm, respectively, which are much higher than those of MHAp. It is noticed that after introducing IBU molecules into MHAp-FL, both the BET surface area and pore volume are remarkably reduced, implying that the mesoporous channels have been filled with IBU. All the textural parameters of the corresponding materials are summarized in Table 1.

The FT-IR spectra of MHAp, MHAp-FL, PATPE, IBU, and MHAp-FL-IBU are displayed in Fig. S2.† The bands at 567 and 603 cm^{-1} can be assigned to the ν_4 bending vibration of P–O bond, and the 961 cm^{-1} band is due to the ν_1 symmetric P–O stretching vibration. The strong bands at 1044 and 1100 cm^{-1} are assigned to the ν_3 stretching vibration of P–O bond. The

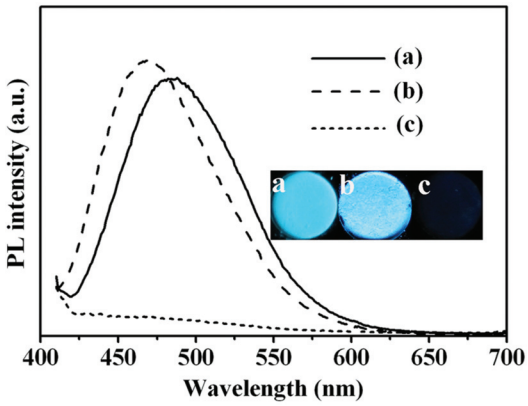

Fig. 5 Fluorescence spectra of (a) MHAp-FL, (b) PATPE, (c) MHAp. Excitation wavelength: 400 nm. Insert photos were taken under the UV light (365 nm).

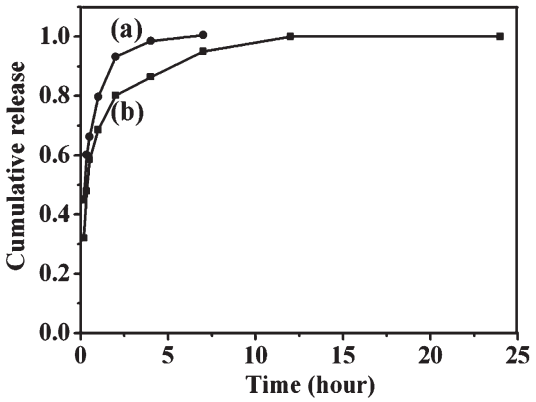

Fig. 6 The release curves of IBU from (a) MHAp-IBU, (b) MHAp-FL-IBU in SBF.

band at 3435 cm^{-1} corresponds to the vibration mode of OH groups, while the peak at 3572 cm^{-1} to the stretching vibration of OH^- ions in the HAp lattice. All the above bands are characteristic for the typical HAp FT-IR spectrum.[31] For MHAp-FL, the new bands appeared between 1400–1600 cm^{-1} can be assigned to the stretching vibration of C=C of aromatic rings (Fig. S2b†), confirming that PATPE was successfully incorporated into the material.[32] Pure IBU (Fig. S2d†) shows a strong band at 1720 cm^{-1}, which is attributed to the vibration of carboxyl group (COOH) present in IBU. It is found that for the IBU loaded MHAp-FL-IBU (Fig. S2e†), the band at 1720 cm^{-1} is still obvious and the IR bands of HAp can also be observed, indicating that IBU has been adsorbed into MHAp-FL and the material can be used as a drug carrier.

The pure MHAp shows no luminescence under the UV irradiation (Fig. 5). However, after the incorporation of PATPE, MHAp-FL emits strong blue luminescence centered at 487 nm, with a little red shift compared to pure PATPE (470 nm). This is because when PATPE molecules were loaded in the framework of MHAp, the internal rotations of the molecules are largely restricted, thus block the nonradiative relaxation channel and populate the radioactive decay to the ground state, making the material emissive. Therefore such bioactive material may be a new candidate for simultaneous drug carrying and cell imaging in potential bioapplications, and this will be further discussed in the next section.

As there are a large number of OH groups on the surface of MHAp-FL, which can form hydrogen bonds with the carboxyl groups, we choose IBU as a drug marker to study the drug loading and release properties of MHAp-FL. It can be seen that MHAp-FL shows much higher drug loading amount (73 wt%) compared to MHAp (24 wt%) due to its higher surface area and larger-sized pore in the hollow ellipsoidal capsule structure (Table 1).

The release behaviors of MHAp-IBU and MHAp-FL-IBU in the SBF are shown in Fig. 6. They both gave an initial burst release of about 50% in the first few minutes which is ascribed to the weak interaction between IBU and the outer surface of MHAp or MHAp-FL. As the time extended, MHAp-FL-IBU showed much slower and sustained release of IBU, which can avoid the explosive release of IBU and prolong the drug effect. The reason can be explained by the formation of hydrogen bonds between $-COO^-$ groups of IBU and –OH groups of MHAp-FL hollow capsules. Meanwhile, the porous texture is also important for slowing down or holding back the release of loaded IBU.

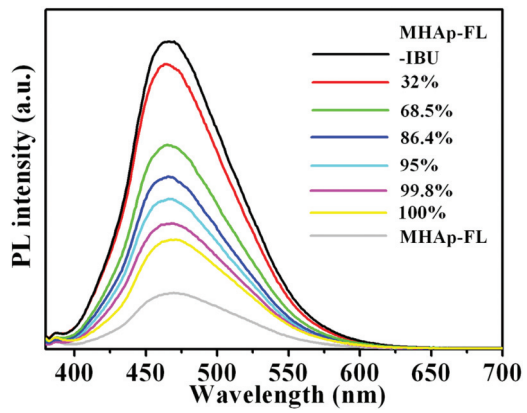

Fig. 7 Fluorescence spectra of MHAp-FL and MHAp-FL-IBU with ibuprofen released at different percentages.

After loaded with IBU, the PL intensity of MHAp-FL-IBU is largely increased compared with MHAp-FL (Fig. 7). This is due to that the intramolecular rotations of the TPE core are further restricted inside the mesopore of MHAp-FL-IBU. Notably, when IBU was released, the PL intensity of MHAp-FL-IBU decreases because the inhibition of AIE molecules rotation is gradually reduced. After the drug release balances, there still remains a certain amount of molecules in the materials, leading to their PL intensity a little higher than that of MHAp-FL. Fig. 8 shows the plot of PL intensity of MHAp-FL-IBU as a function of cumulative release amount of ibuprofen. Other drugs, such as metoprolol, gentamycin sulfate, were also attempted for the adsorption in MHAp-FL, all of which showed enhanced fluorescence (Fig. 9). Notice that the increase of PL intensity of MHAp-FL loaded with metoprolol is

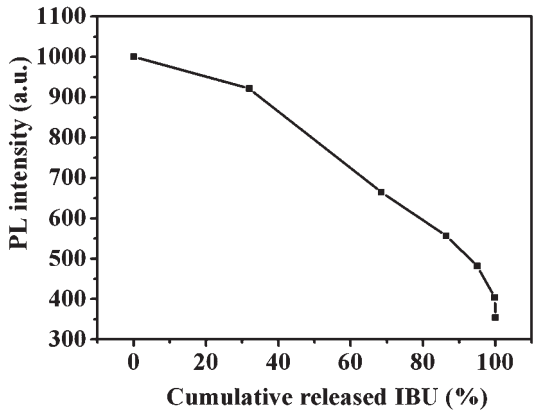

Fig. 8 The plot of PL intensity of MHAp-FL-IBU as a function of cumulative release amount of ibuprofen.

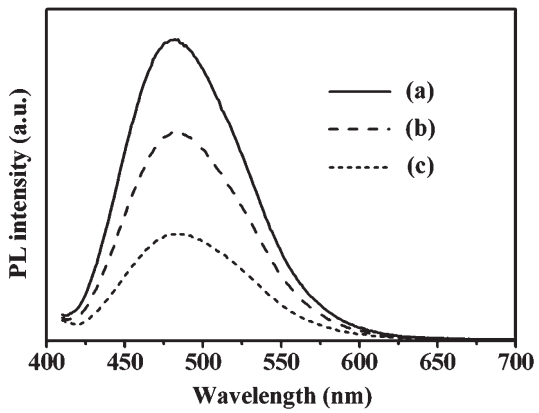

Fig. 9 Fluorescence spectra of MHAp-FL after adsorption of (a) metoprolol, (b) gentamycin sulfate, (c) MHAp-FL. Excitation wavelength: 400 nm.

higher than that with gentamycin sulfate. This is due to the smaller molecular structure of metoprolol, which can be easily adsorbed into the materials. Above studies indicate that the AIE functionalized mesoporous materials may have the potential application as drug delivery and can be further used to track and monitor the drug release in terms of the change of PL intensity in future bioapplications.

To further evaluate MHAp-FL that can be potentially applied as an effective drug delivery system, *in vitro* cytotoxicity against HUH7 human hepatoma cells was investigated by the MTT assay to determine the toxicity of biomaterials based on the formation of dark-red formazan by the metabolically active cells. After the extract solutions of MHAp-FL incubated with HUH7 human hepatoma cells for 24 h, the cell viabilities were above 95% even when the concentration of the extract solution was about 40 mg mL^{-1} (Fig. 10). As a comparison, the viabilities of HUH7 human hepatoma cells incubated with MHAp at different concentrations were also studied. The above experimental results demonstrate that the AIE luminogen functionalized mesoporous HAp has good biocompatibility as with MHAp, which is an important prerequisite for imaging guided carriers for bioapplications.

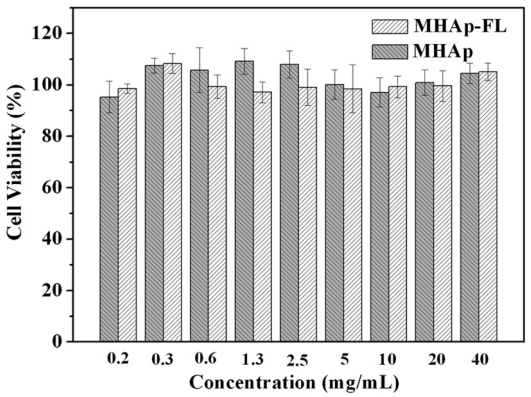

Fig. 10 Cell viabilities of HUH7 human hepatoma cells incubated with the extract solutions of MHAp and MHAp-FL at different concentrations.

4. Conclusions

In summary, organophosphonic acid (PATPE) based on AIE-active tetraphenylethene has been synthesized and its ester derivative shows the characteristic AIE property in DMSO–H_2O solution. Then PATPE was incorporated into HAp *via* P–O–Ca covalent bonds by a co-condensation approach forming ellipsoidal hollow nanocapsules. The as-prepared AIE luminogen bridged mesostructured hydroxyapatite (MHAp-FL) exhibits strong blue luminescence and good biocompatibility, and shows a high IBU storage capacity and favorable drug release behavior compared to pure MHAp. More importantly, the fluorescence intensity changes with the amount of drug molecules adsorbed to the materials, suggesting that the drug release may be tracked and monitored by the change of luminescence intensity. The multifunctionality of the materials presented here offers new opportunities for the simultaneous bioimaging and drug transports in potential bioapplications. Although the resultant materials are excited by UV light, which may limit their practical application in drug delivery systems, this study provides a general concept for designing multifunctional bioactive materials for applications. Further work in developing such materials with long-wavelength emission is undergoing.

Acknowledgements

This work is supported by the National Natural Science Foundation of China and the State Basic Research Project (Grant: 2011CB808703) of China.

Notes and references

1 M. Vallet-Regí, A. Rámila, R. P. del Real and J. Pérez-Pariente, *Chem. Mater.*, 2001, **13**, 308.
2 M. Hartmann, *Chem. Mater.*, 2005, **17**, 4577.
3 I. I. Slowing, B. G. Trewyn, S. Giri and V. S.-Y. Lin, *Adv. Funct. Mater.*, 2007, **17**, 1225.
4 Z. X. Wu and D. Y. Zhao, *Chem. Commun.*, 2011, **47**, 3332.

5 A. Schlossbauer, C. Dohmen, D. Schaffert, E. Wagner and T. Bein, *Angew. Chem., Int. Ed.*, 2011, **50**, 6828.
6 N. Sahiner, C. Silan, S. Sagbas, P. Ilgin, S. Butun, H. Erdugan and R. S. Ayyala, *Microporous Mesoporous Mater.*, 2012, **155**, 124.
7 J. L. Gu, S. S. Su, Y. S. Li, Q. J. He and J. L. Shi, *Chem. Commun.*, 2011, **47**, 2101.
8 S. H. Tang, X. Q. Huang, X. L. Chen and N. F. Zheng, *Adv. Funct. Mater.*, 2010, **20**, 2442.
9 L. L. Hench and J. Wilson, *Science*, 1984, **226**, 630.
10 M. Y. Ma, Y. J. Zhu, L. Li and S. W. Cao, *J. Mater. Chem.*, 2008, **18**, 2722.
11 P. P. Yang, Z. W. Quan, C. X. Li, X. J. Kang, H. Z. Lian and J. Lin, *Biomaterials*, 2008, **29**, 4341.
12 M. Liong, S. Angelos, E. Choi, K. Patel, J. F. Stoddart and J. I. Zink, *J. Mater. Chem.*, 2009, **19**, 6251.
13 S. Jiang, M. K. Gnanasammandhan and Y. Zhang, *J. R. Soc. Interface*, 2010, **7**, 3.
14 X. G. Hu, P. Zrazhevskiy and X. H. Gao, *Ann. Biomed. Eng.*, 2009, **37**, 1960.
15 I. Díez and R. H. A. Ras, *Nanoscale*, 2011, **3**, 1963.
16 Z. H. Xu, Y. Gao, S. S. Huang, P. A. Ma, J. Lin and J. Y. Fang, *Dalton Trans.*, 2011, **40**, 4846.
17 J. Kim, H. S. Kim, N. Lee, T. Kim, H. Kim, T. Yu, I. C. Song, W. K. Moon and T. Hyeon, *Angew. Chem., Int. Ed.*, 2008, **47**, 8438.
18 J. E. Lee, N. Lee, H. Kim, J. Kim, S. H. Choi, J. H. Kim, T. Kim, I. C. Song, S. P. Park, W. K. Moon and T. Hyeon, *J. Am. Chem. Soc.*, 2010, **132**, 552.
19 A. M. Derfus, W. C. W. Chan and S. N. Bhatia, *Nano Lett.*, 2004, **4**, 11.
20 S. W. Thomas III, G. D. Joly and T. M. Swager, *Chem. Rev.*, 2007, **107**, 1339.
21 J. D. Luo, Z. L. Xie, J. W. Y. Lam, L. Cheng, H. Y. Chen, C. F. Qiu, H. S. Kwok, X. W. Zhan, Y. Q. Liu, D. B. Zhu and B. Z. Tang, *Chem. Commun.*, 2001, 1740.
22 Y. N. Hong, J. W. Y. Lam and B. Z. Tang, *Chem. Soc. Rev.*, 2011, **40**, 5361.
23 Z. Li, Y. Q. Dong, B. X. Mi, Y. H. Tang, M. Hälussler, H. Tong, Y. P. Dong, J. W. Y. Lam, Y. Ren, H. H. Y. Sung, K. S. Wong, P. Gao, I. D. Williams, H. S. Kwok and B. Z. Tang, *J. Phys. Chem. B*, 2005, **109**, 10061.
24 F. Mahtab, Y. Yu, J. W. Y. Lam, J. Z. Liu, B. Zhang, P. Lu, X. X. Zhang and B. Z. Tang, *Adv. Funct. Mater.*, 2011, **21**, 1733.
25 D. Wang, J. Qian, S. L. He, J. S. Park, K. S. Lee, S. H. Han and Y. Mu, *Biomaterials*, 2011, **32**, 5880.
26 M. Wang, G. X. Zhang, D. Q. Zhang, D. B. Zhu and B. Z. Tang, *J. Mater. Chem.*, 2010, **20**, 1858.
27 D. D. Li, J. H. Yu and R. R. Xu, *Chem. Commun.*, 2011, **47**, 11077.
28 D. D. Li, J. Z. Liu, R. T. K. Kwok, Z. Q. Liang, B. Z. Tang and J. H. Yu, *Chem. Commun.*, 2012, **48**, 7167.
29 A. J. Qin, L. Tang, J. W. Y. Lam, C. K. W. Jim, Y. Yu, H. Zhao, J. Z. Sun and B. Z. Tang, *Adv. Funct. Mater.*, 2009, **19**, 1891.
30 E. Boanini, M. Gazzano, K. Rubini and A. Bigi, *Adv. Mater.*, 2007, **19**, 2499.
31 J. Andersson, S. Areva, B. Spliethoff and M. Lindén, *Biomaterials*, 2005, **26**, 6827.
32 E. Fuente, J. A. Menéndez, M. A. Díez, D. Suárez and M. A. Montes-Morán, *J. Phys. Chem. B*, 2003, **107**, 6350.